Liquid Crystal Elastomers with Mechanical Properties of a Muscle

Donald L. Thomsen III,[†] Patrick Keller,[‡] Jawad Naciri, Roger Pink,[§] Hong Jeon, Devanand Shenoy, and Banahalli R. Ratna*

Center for Bio/Molecular Science and Engineering, Naval Research Laboratory, 4555 Overlook Avenue SW, Code 6900, Washington, D.C. 20375

Received September 22, 2000; Revised Manuscript Received May 15, 2001

ABSTRACT: Free-standing anisotropic side chain liquid crystalline elastomer films have been prepared using mesogens with laterally affixed polymerizable side chains. We present data on two networks: one containing the monomer of 4′-acryloyloxybutyl 2,5-(4′-butyloxybenzoyloxy)benzoate and another from a 50/50 mol % mixture of the above with 4′-acryloyloxybutyl 2,5-di(4′-pentylcyclohexyloyloxy)benzoate. The cross-linking was achieved using 10 mol % of 1,6-hexanediol diacrylate. The calculated cross-linking density, as determined from the Young's modulus, was in the 10^{-5} mol/cm^3 range. Thermoelastic responses show strain changes through the nematic−isotropic phase transition to be 30−45%. The order parameters of the oriented films were determined from the dichroic ratio of IR absorption at 3343 cm^{-1} to the in-plane aromatic stretching overtone of the LC mesogen core. The variation of the order parameter with temperature scales similar to the strain changes at constant stress. Isostrain studies, conducted through the nematic to isotropic phase transition, show that the two networks behave as true elastomers with significant differences in the force developed. Dynamic shear measurements near the nematic to isotropic phase transition region show that the mechanical relaxation peak appears above 100 Hz, and that viscoelastic relaxations are minimal in the nematic to isotropic phase transition region below 5−10 Hz.

Intoduction

Skeletal muscles are anisotropic, exhibiting contraction/elongation along the fiber axis. The rate at which a muscle can work is limited by three variables: the strain through which it can shorten, the stress which it can exert, and the contraction frequency.[1] The values of these three variables, on an average, are 25%, 350 kPa, and 5−10 Hz, respectively. There have been a number of efforts to develop artificial muscle-like materials. These include piezoelectrics,[2] Ni−Ti alloys,[3] conducting polymers,[4−6] electrostrictive polymers,[7] carbon nanotube films,[8] and hydrogels.[9] These actuator materials provide a wide range of stress, strain, and response compared to the case of skeletal muscles.[10] The possibility of using a liquid crystal elastomer (LCE)[11] as an artificial muscle was first suggested by de Gennes.[12] Liquid crystalline elastomers (LCEs), which have been the subject of a number of reviews,[13−17] have been shown to change dimensions under low stresses[18,19] through phase transitions and retain network memory.[20] Therefore, an ordered LCE with its anisotropic properties can provide an excellent framework to mimic muscular action.

The coupling between the liquid crystal side chain and the backbone is critical to the thermostrictive behavior of LCE materials. This coupling is strong when the length of the spacer between the liquid crystalline mesogen and the polymer backbone is short. Neutron scattering studies of a liquid crystalline lateral side chain polymer have shown that for short spacer lengths the orientational order of the mesogens induces backbone anisotropy,[21−27] the radius of gyration having a prolate extended shape with a shape anisotropy of 5:1 in the nematic phase. In contrast, the radius of gyration is spherical in the isotropic phase. The polymer chains between cross-links in an elastomer can undergo similar conformational changes. Since the elastomer is a solid and cannot flow, the conformational change leads to a shape change which is thermally reversible. We have chosen to study elastomers with laterally affixed liquid crystal mesogens, since they have been shown to exhibit large backbone anisotropy. In this paper, we show that the stress, strain, and the strain rate exhibited by a laterally attached side chain liquid crystal elastomer across the nematic−isotropic phase transition can be comparable to that of a skeletal muscle.

Experimental Section

Materials and Techniques. 2,5-Dihydroxybenzoic acid, benzyl bromide, 4-pentylcyclohexylcarboxylic acid, 4-hydroxybutyl acrylate, and anhydrous dichloromethane were obtained from Aldrich and used without further purification. 1,6-Hexanediol diacrylate was purchased from Scientific Polymer with MEHQ inhibitor which was removed using an inhibitor removal column prior to use. Irgacure 369 from Ciba-Geigy was used at a concentration of 0.1 mol % with respect to monomer concentrations. Analytical TLC was conducted on Whatman precoated silica gel 60-F254 plates. The 400 MHz ^{1}H NMR spectra were recorded on a Bruker DRX-400 spectrometer. All spectra were run in $CDCl_3$ solution.

Thermal Analysis. A Perkin-Elmer differential scanning calorimeter DSC 7 equipped with a CCA 7 liquid nitrogen cooling accessory was used to study the nematic−isotropic phase transtion of the monomers and their corresponding elastomers. Scans were done at 3 °C/min heating and cooling rate over a temperature range of −5 to 180 °C. The samples were first heated to 150 °C and quenched to the block temperature of −60 °C before running the scans. The melting temperature of indium was used as a standard for temperature calibration which agreed to within 1 deg of the expected value.

FTIR. A Nicolet Magna FTIR 760 series II with DTGS detector and equipped with a ZnSe crystal polarizer was used

[†] Currently at NASA Langley Research Center, Hampton, VA 23681-0001.

[‡] Laboratoire Physico-Chimie Curie, CNRS-UMR 168, Institut Curie-Section de Recherche, 11, rue P et M Curie, 75231 Paris Cedex 05, France.

[§] George Mason University, 4400 University Drive, Fairfax, VA 22030-4444.

* Corresponding author.

10.1021/ma001639q CCC: $20.00
Published on Web 07/13/2001

for data acquisition between 4000 and 600 cm^{-1} using 4 cm^{-1} resolution and 32 scans. Polarized FTIR of the aligned monomer (**4a**) was done in a NaCl cell having 180° C rubbed polyimide surfaces with 50 μm Mylar spacers. The monomer (**4a**) was vacuum-filled at 85 °C and aligned on cooling to room temperature over a 1 h period. The scans were done at room temperature in the supercooled nematic state. The LCE films were placed between NaCl plates for the experiments. The spectra were collected in both the nematic and isotropic phases after stabilizing the temperature for 5 min before each scan using an Instec hot stage temperature controller equipped with a thermistor.

Mechanical Studies. All measurements were done on a TA Instrument DMA 2980 with tension clamp for static stress/strain, isostrain, and thermoelastic measurements and shear sandwich clamp for dynamic measurements. A stress/strain measurement was done in the rubbery plateau at a strain rate of 0.05 N/min. Thermoelastic experiments were done on both heating and cooling cycles at a number of constant applied stresses after an initial 3 min isothermal hold before increasing the stress. Isostrain measurements were done on the elastomer films heating through the nematic−isotropic phase transition at 0.5 °C/min with the films held under a small preload stress and a 5% strain. Dynamic mechanical analysis was done in a shear sandwich clamp with the shear direction parallel to the rubbing direction. Isothermal frequency sweeps were done between 200 and 0.1 Hz at 15 μm amplitude at 5 °C steps on cooling from 142.5 to 102.5 °C. The method of the shear sandwich experiment does not include the compressive force holding the sample together, which would effect the G' and G'' values but not the ratio, tan δ. The sample temperature was allowed to stabilize for 3 min before each frequency sweep.

Synthesis. Typical procedures of the synthesis of the materials are described below.

Benzyl 2,5-Dihydroxybenzoate (**1**). To a stirred solution of 2,5-dihydroxybenzoic acid (6.16 g, 40 mmol) in DMF (60 mL) was added solid $NaHCO_3$ (9.9 g, 117 mmol). The mixture was heated and stirred at 70 °C for 1 h. Benzyl bromide (6.84 g, 40 mmol) was added, and the mixture was heated for 7 h. The reaction mixture was cooled, diluted with water (200 mL), and extracted twice with 100 mL of a 50:50 hexane/ethyl acetate mixture. The organic phases were washed twice with water (100 mL) and dried over Na_2SO_4. After evaporation of the solvents, the residue was subjected to column chromatography on silica gel with diethyl ether as eluting solvent to yield 9 g (92%) of viscous oil which crystallizes on standing. ^{1}H NMR ($CDCl_3$, TMS) δ (ppm): 4.8 (broad s, 2H, OH), 5.3 (s, 2H, CH_2−O), 6.99−7.10 (m, 2H, ArH), 7.4 (s, 1H, ArH), 7.42−7.5 (m, 5H, ArH). Elemental analysis: calculated for $C_{14}H_{12}O_4$: C, 68.85; H, 4.95. Found: C, 68.77; H, 4.90.

Benzyl 2,5-Di(4′-butyloxybenzoyloxy)benzoate (**2a**). A solution of benzyl 2,5-dihydroxybenzoate (**1**) (6 g, 24.6 mmol), 4-butyloxybenzoic acid (10.5 g, 54 mmol), *N*,*N*-dicyclohexylcarbodiimide (11.14 g, 54 mmol), and pyrrolidinopyridine (0.8 g, 5.4 mmol) in 400 mL of dichloromethane was stirred at room temperature for 12 h. The *N*,*N*-dicyclohexyl urea was filtered and the filtrate was washed with water (150 mL), 5% acetic acid solution (150 mL), and water (150 mL) and dried over Na_2SO_4. After evaporation of the solvent, the crude product was recrystallized (3×) from ethanol to yield 12.31 g (84%). ^{1}H NMR ($CDCl_3$, TMS) δ (ppm): 1.0 (t, 6H, $-CH_3$), 1.5 (m, 4H, $-CH_2-$), 1.8 (m, 4H, $-CH_2-$), 4.01 (t, 4H, $-CH_2-$O), 5.2 (s, 2H, $-CH_2-$O), 7.0−7.1 (m, 4H, ArH), 7.3−7.45 (m, 7H, ArH), 7.9 (s, 1H, ArH), 8.14−8.18 (m, 4, ArH). Elemental analysis: calculated for $C_{36}H_{36}O_8$: C, 72.47; H, 6.08. Found: C, 72.35; H, 6.12.

2,5-Di(4′-butyloxybenzoyloxy)benzoic Acid (**3a**). Hydrogen was allowed to bubble through a stirred suspension of 10% palladium on carbon (3 g) in 800 mL of dichloromethane. After 15 min 12.3 g (20.6 mmol) of the benzyl ether **2a** was added, and the reaction mixture was stirred overnight. The reaction was monitored by TLC (50:50 hexane/ethyl acetate). After filtration on Celite pad, the solvent was evaporated, and the product (9.6 g, 92%) was dried under vacuum. ^{1}H NMR ($CDCl_3$, TMS) δ (ppm): 1.06 (t, 6H, $-CH_3$), 1.55 (m, 4H, $-CH_2$), 1.84 (m, 4H, $-CH_2-$), 4.02 (m, 4H, $-O-CH_2$), 7.0−7.2 (m, 4H, ArH), 7.3−7.5 (m, 2H, ArH), 7.9 (s, 1H, ArH), 8.15−8.3 (m, 4H, ArH). Elemental analysis: calculated for $C_{29}H_{30}O_8$: C, 68.76; H, 5.97. Found: C, 68.70; H, 6.0.

(4″-Acryloyloxybutyl) 2,5-Di(4′-butyloxybenzoyloxy)benzoate (**4a**). A solution of 2,5-di(4′-butyloxybenzoyloxy)benzoic acid (**3a**) (9.6 g, 18.9 mmol), 4-hydroxybutyl acrylate (3 g, 20.8 mmol), *N*,*N*-dicyclohexylcarbodiimide (4.3 g, 20.8 mmol), and 4-pyrrolidinopyridine (0.3 g, 2.02 mmol) in 300 mL of dichloromethane was stirred overnight at room temperature. The *N*,*N*-dicyclohexylurea was filtered, and the filtrate washed with water (100 mL), 5% acetic acid solution (100 mL), and water (100 mL) and dried over Na_2SO_4. The solvent was evaporated, and the crude product was recrystallized (3×) from ethanol. Yield: 9 g, 75%. ^{1}H NMR ($CDCl_3$, TMS) δ (ppm): 1.0 (t, 6H, $-CH_3$), 1.5−1.7 (m, 8H, $-CH_2-$), 1.82 (m, 4H, $-CH_2-$), 4.02−4.15 (m, 6H, $-OCH_2$), 4.2 (t, 2H, OCO$-CH_2$), 5.8 (m, 1H, CH_2═C), 6.1 (m, 1H, C═CH−), 6.35 (m, 1H, CH_2═C), 7.0−7.2 (m, 4H, ArH), 7.3−7.5 (m, 2H, ArH), 7.9 (s, 1H, ArH), 8.2−8.3 (m, 4H, ArH). Elemental analysis: calculated for $C_{36}H_{40}O_{10}$: C, 68.34; H, 6.37. Found: C, 68.25; H, 6.30. FTIR (cm^{-1}, neat): 3434, 3340, 3207, 3154, 3103, 3079, 3051, 2961, 2935, 2874, 2767, 2633, 2574, 2517, 2407, 2105, 2040, 2016, 1935, 1724, 1636, 1603, 1581, 1510, 1489, 1471, 11393, 1319, 1275, 1243, 1168, 1141, 1070, 1030, 1006, 983, 970, 950, 909, 876, 849, 811, 789, 773, 763, 744, 692, 671, 645, 630, 618.

Benzyl 2,5-Di(4′-pentylcyclohexylcarboxyloxy)benzoate (**2b**). A solution of benzyl 2,5-dihydroxybenzoate (**1**) (2.44 g, 10 mmol), 4-pentylcyclohexylcarboxylic acid (4.36 g, 22 mmol), *N*,*N*-dicyclohexylcarbodiimide (4.53 g, 22 mmol), and 4-pyrrolidinopyridine (0.32 g, 2.2 mmol) in 100 mL of dichloromethane was stirred for 12 h at room temperature. The *N*,*N*-dicyclohexylurea was filtered, and the filtrate was washed with water (100 mL), 5% acetic acid solution (100 mL), and water (100 mL) and dried over Na_2SO_4. The solvent was evaporated, and the crude product was recrystallized twice from ethanol. Yield: 5 g, 82%. ^{1}H NMR ($CDCl_3$, TMS) δ (ppm): 0.92 (t, 6H, $-CH_3$), 1.05 (m, 4H, −CH (EQ)), 1.19 (m, 16H, $-CH_2$), 1.2 (m, 2H, −CH (AX)), 1.3 (m, 4H, −CH (EQ)), 1.95 (m, 4H, −CH (EQ)), 2.2 (m, 4H, −CH (AX)), 2.51 (m, 2H, −CH (AX)), 5.3 (s, 2H, $-OCH_2$), 7.1 (m, 1H, ArH), 7.28 (m, 1H, ArH), 7.4 (m, 5H, ArH), 7.81 (s, 1H, ArH). Elemental analysis: calculated for $C_{38}H_{52}O_6$: C, 75.46; H, 8.67. Found: C, 75.40; H, 8.70.

2,5-Di(4′-pentylcyclohexylcarboxyloxy)benzoic Acid (**3b**). Hydrogen was allowed to bubble through a stirred suspension of 10% palladium on carbon (0.5 g) in 300 mL of dichloromethane. After 15 min, 4.8 g (7.9 mmol) of the benzyl ether **2b** was added, and the reaction mixture was stirred overnight. The reaction was monitored by TLC (50:50 hexane/ethyl acetate). After filtration on Celite pad, the solvent was evaporated, and the product (4 g, 97%) was dried under vacuum. ^{1}H NMR ($CDCl_3$, TMS) δ (ppm): 0.9 (t, 6H, $-CH_3$), 1.0 (m, 4H, −CH (EQ)), 1.18 (m, 16H, $-CH_2$), 1.2 (m, 2H, −CH (AX)), 1.3 (m, 4H, −CH (EQ)), 1.9 (m, 4H, −CH (EQ)), 2.2 (m, 4H, −CH (AX)), 2.52 (m, 2H, −CH (AX)), 7.1 (m, 1H, ArH), 7.3 (m, 1H, ArH), 7.8 (s, 1H, ArH). Elemental analysis: calculated for $C_{31}H_{46}O_6$: C, 72.34; H, 9.01. Found: C, 72.25; H, 8.91.

(4″-Acryloyloxybutyl) 2,5-Di(4′-pentylcyclohexylcarboxyloxy)benzoate (**4b**). A solution of **3b** (3.8 g, 7.39 mmol), 4-hydroxybutyl acrylate (1.17 g, 8.13 mmol), *N*,*N*-dicyclohexylcarbodiimide (1.68 g, 8.15 mmol), and pyrrolidinopyridine (0.12 g, 0.81 mmol) in 150 mL of dichloromethane was stirred overnight at room temperature. The *N*,*N*-dicyclohexylurea was filtered, and the filtrate was washed with water (100 mL), 5% acetic acid solution (100 mL), and water (100 mL) and dried over Na_2SO_4. The solvent was evaporated to yield very viscous oil. The product was purified by crystallization from ethanol (3×). Yield: 2.03 g, 43%. ^{1}H NMR ($CDCl_3$, TMS) δ (ppm): 0.9−1.1 (m, 10H, −CH (EQ)), $-CH_3$), 1.2−1.4 (m, 14H, −CH (AX)), $-CH_2-$), 1.5−1.6 (m, 8H, $-CH_2-$), 1.75−1.9 (m, 8H, −CH (AX, EQ)), 2.1 (m, 4H, −CH (AX)), 2.18 (m, 4H, −CH (AX)), 2.51 (m, 2H, −CH (AX)), 4.2 (t, 2H, $-CH_2-$OCO), 4.3 (t, 2H, OCO$-CH_2$), 5.8 (m, 1H, CH_2═C), 6.12 (m, 1H, C═CH−), 6.4 (m, 1H, CH_2═C), 7.1 (m, 1H, ArH), 7.3 (m, 1H, ArH), 7.75 (s, 1H, ArH).

Scheme 1. Liquid Crystal Monomer Synthesis, 4″-Acryloyloxybutyl 2,5-Di(4′-butyloxybenzoyloxy)benzoate 4a

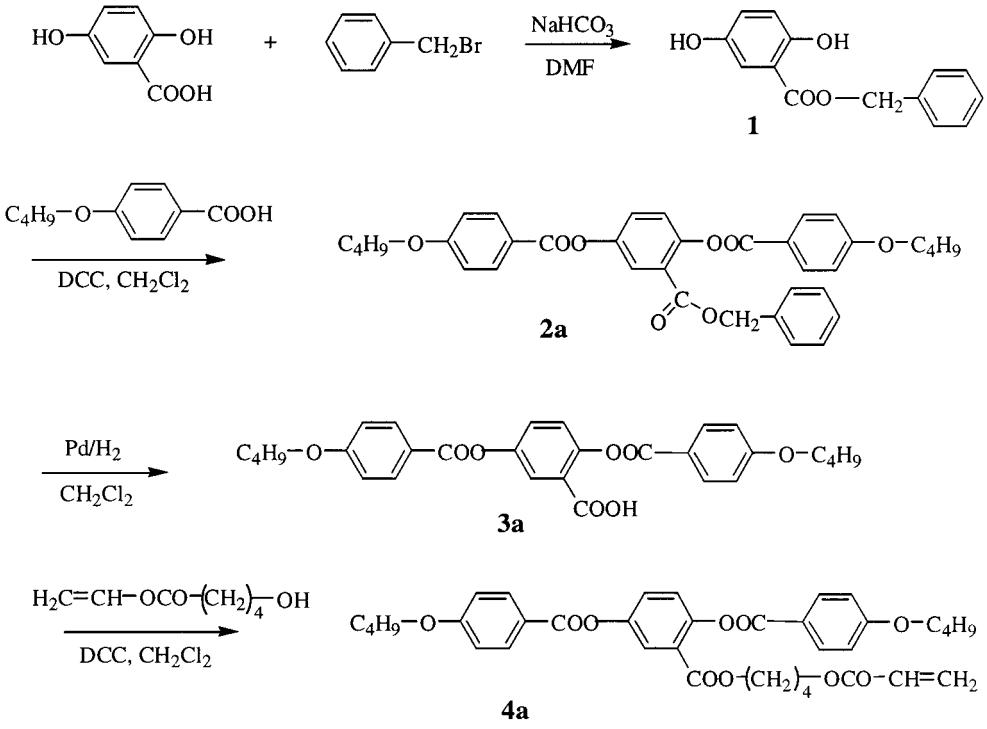

Scheme 2. Liquid Crystal Monomer Synthesis, 4″-Acryloyloxybutyl 2,5-Di(4′-pentylcyclohexylcarboxyloxy)benzoate 4b

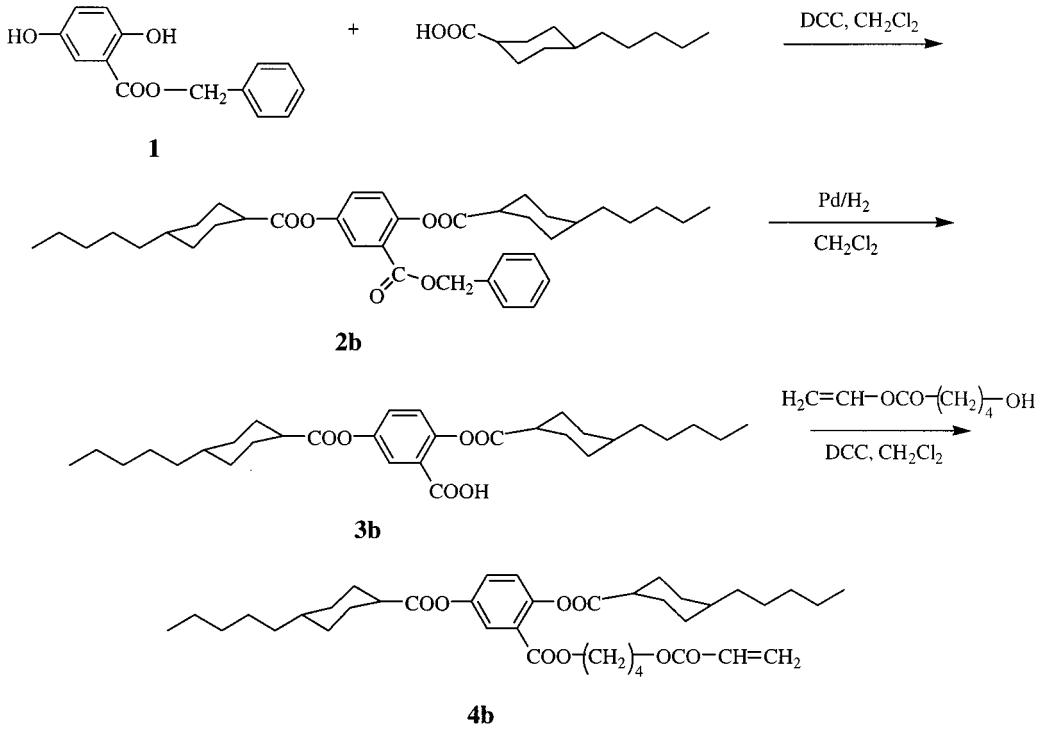

Elemental analysis: calculated for $C_{38}H_{56}O_8$: C, 71.22; H, 8.81. Found: C, 71.16; H, 8.71.

Anisotropic LCE Film Preparation. Monomers **4a** and **4b**, whose chemical structures are shown in Schemes 1 and 2, were prepared according to methods detailed above. 90 mol % (**4a**) and 10 mol % 1,6-hexanediol diacrylate was used for the preparation of aligned LCE 1. A mixture of **4a** and **4b** at a 45/45 mol % ratio was used with 10 mol % 1,6-hexanediol diacrylate for the preparation of aligned LCE 2. Samples were filled in rubbed poly(vinyl alcohol) (PVA)-coated glass cells of 50 and 100 μm gap under 25 mmHg vacuum at 85 °C. The filled cells were heated to 95 °C and cooled at −1 °C/min in to the nematic phase to achieve alignment. The cooling was carried out under yellow light and nitrogen to prevent polymerization in the isotropic phase. The polymerization temperature was 75 °C for LCE 1 30 °C for LCE 2. Photopolymerization was accomplished with a 5 min light exposure of 0.97 mW using a 75 W Oriel xenon UV lamp equipped with a 365 nm cutoff filter. Free-standing films were obtained by opening cells following heating in distilled water at 80−100 °C for 20 min. FTIR (cm^{-1}) (NaCl disks, 50 μm films for LCE1 and LCE2) LCE1: 3447, 3340, 3208, 3155, 3076, 2927, 2874, 2764, 2577, 2515, 2106, 2015, 1917, 1740, 1607, 1578, 1508, 1489, 1472, 1465, 1457, 1436, 1420, 1387, 1362, 1246, 1174, 1081,

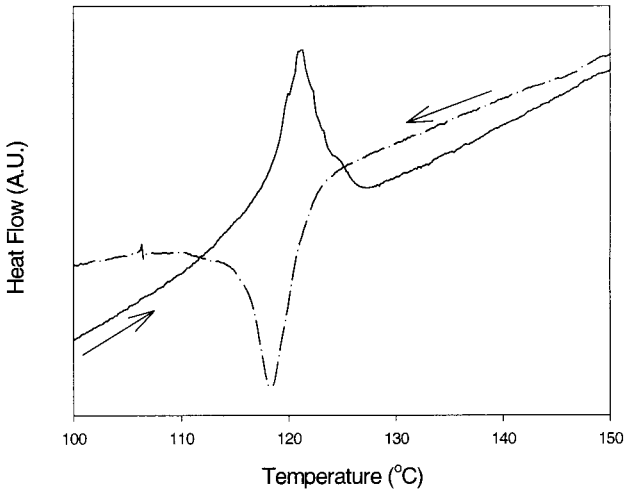

Figure 1. DSC scans of LCE 1 on heating and cooling cycles at 3 °C/min rate.

Table 1. Phase Transition Temperatures of Materials Studied As Determined from DSC

material	T_g (°C)	T_{IN} (°C)	**4a** (mol %)	**4b** (mol %)	cross-linker (mol %)
LCE 1	39.9	119.3		90	10
LCE 2	18.8	85.8	45	45	10
4a	71.9 (T_{KN})	98.3			
4b	74.0 (T_{KI})	42.2			

1006, 970, 908, 879, 847, 812, 762, 692, 643, 630, 617. LCE2: 3493, 3444, 3343, 3208, 3155, 3077, 3051, 2956, 2920, 2871, 2857, 2635, 2575, 2517, 2105, 2030, 1914, 1740, 1605, 1580, 1510, 1489, 1467, 1451, 1422, 1389, 1378, 1302, 1250, 1150, 1074, 1031, 1007, 973, 927, 911, 903, 880, 847, 811, 762, 692, 643, 630, 618.

Results and Discussion

Phase transition behavior of the monomers and elastomers was characterized by DSC. The phase transition temperatures on cooling are given in Table 1 along with the chemical composition of the elastomers. The I−N transition of **4b** is monotropic. The glass transition temperature (T_g) is higher for LCE 1 than LCE 2. This we believe is due the presence of monomer **4b** with flexible cyclohexyl groups. The I−N phase transition temperature and the change in enthalpy at this phase transition are lower for LCE 2 than LCE 1 for the same reason, −1.8 vs −2.9 J/g, respectively. Shown in Figure 1 are the DSC scans at 3 °C/min of LCE 1 on heating and cooling cycles.

Stress vs strain plots for the two elastomers, measured along the optic axis of the film, are shown in Figure 2. The measurement was done for LCE 1 in the rubbery plateau at 100 °C at a strain rate of 0.05 N/min, 5.2 kPa preload stress, and a film cross-sectional area of 0.191 mm^2. The measurement of LCE 2 was done at 85 °C at a strain rate of 0.05 N/min 18 kPa preload stress and a film cross-sectional area of 0.111 mm^2. The Young's modulus (E) of 0.40 and 0.88 MPa respectively for LCE 1 and LCE 2 was calculated from the initial slope at small stress values. These values of Young's moduli are characteristic of elastomers. The initial lower slope of the stress−strain curve, especially for LCE1, is probably indicative of the existence of "soft elasticity"[17] at low strain values. As discussed later, the IR dichroic studies on the elastomer films under no load conditions show that the orientational order in these elastomer films are low. A definitive confirmation of the soft elastic behavior can only be made by measuring the order parameter in situ in the DMA, a capability which we do not have at the present time. The cross-linking density n of the films was estimated at low strain values, assuming the samples to be in the rubbery plateau region, using the equation $E = 3nRT$, where E is Young's modulus, R is gas constant, and T is temperature. The calculated cross-linking density of 4.26 $\times$ 10^{-5} and 9.41 $\times$ 10^{-5} mol/cm^3 for the LCE 1 and LCE 2 is lower than the 2.01 $\times$ 10^{-4} mol/cm^3 expected for the 10 mol % of cross-linker used. This may be due to all cross-linking groups not actively participating in the network.

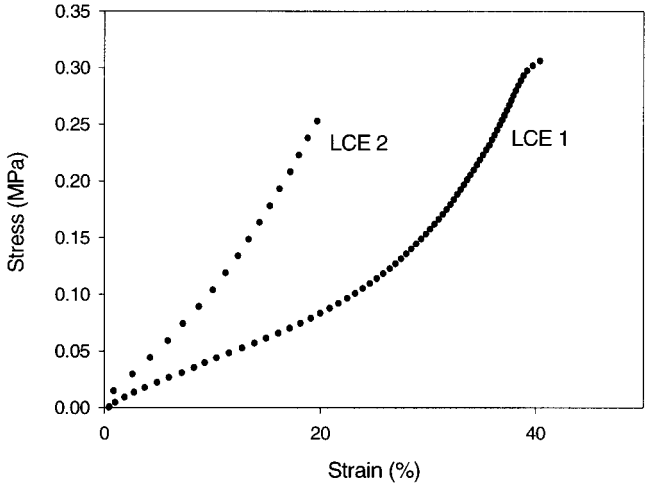

Figure 2. Stress vs strain for LCE 1 and LCE 2. Measurement for LCE 1 was done at 100 °C with a preload stress of 5.2 kPa. Measurement for LCE 2 was done at 85 °C with a preload stress of 18 kPa. The stress was varied at a rate of 0.05 N/min.

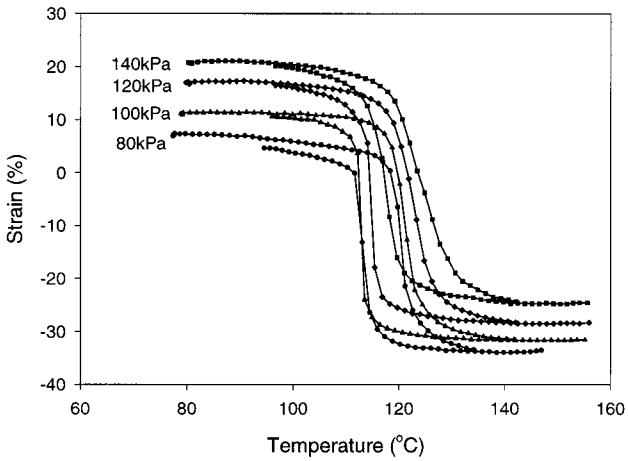

Figure 3. Thermoelastic measurements of aligned LCE 1 at 3 °C/min heating and cooling.

Thermoelastic studies done on both heating and cooling cycles at 3 °C/min rate are shown in Figure 3 for LCE 1. The strain was measured as a function of temperature at constant applied stress over a temperature range covering the nematic to isotropic phase transition. The length of the film remains constant at the lowest temperatures measured in the nematic phase and starts to slowly decrease as the isotropic phase is approached. At the nematic to isotropic phase transition, a sharp decrease in length of ∼40% is observed followed by a slow decrease into the isotropic phase. On cooling, the process is reversed with a sharp increase in length

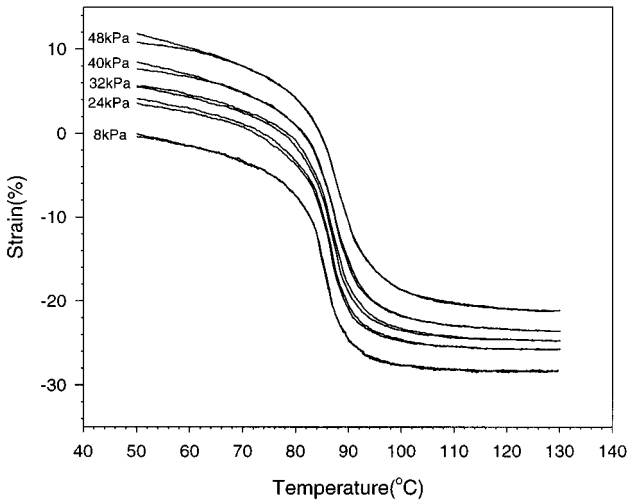

Figure 4. Thermoelastic measurements of aligned LCE 2 at 0.5 °C/min heating and cooling.

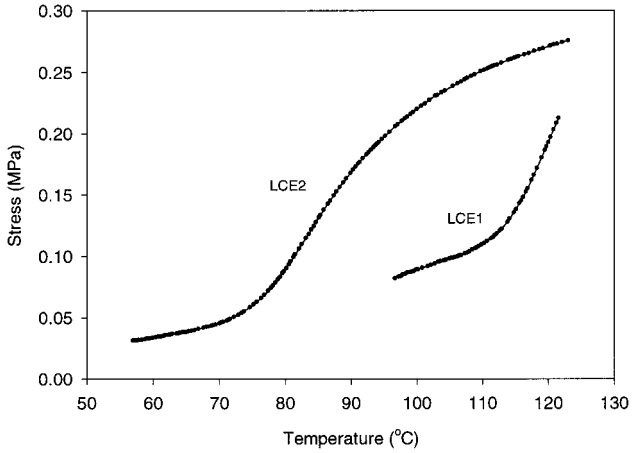

Figure 5. Isostrain measurement at ~5% strain on heating the sample through the nematic to isotropic phase transition for LCE 1 and LCE 2. The preload stress of 62 and 30 kPa were applied respectively on LCE 1 and LCE 2.

on going from the isotropic to nematic phase. The observed hysteresis in temperature may be due to the first order nature of the transition. However, a small temperature lag between the sample and the thermocouple, which may result in an apparent hysteresis, cannot be ruled out. After a heating/cooling cycle, the temperature was held constant for 3 min before increasing the stress value, and the cycle was repeated. The upward shift of the curves with increasing applied stress is due to the increase in length on stretching. Only minor changes were observed in the induced strain. However, an increase was observed in the temperature at which the contraction/extension occurs which may be due to the increased order in the film on stretching. Figure 4 shows the thermoelastic plots near NI for LCE 2. In this case the data were collected at a heating and cooling rate of 0.5 °C. At this heating/cooling rate the sample is in thermal equilibrium with its surroundings. Under these conditions, no hysteresis was observed in LCE 2.[28] The contraction observed in LCE 2 is ~30−35%.

Previous work by Keller et al. has shown that the anisotropy of the backbone of a laterally affixed liquid crystalline side chain polymer decreased as the coupling length increased.[22] A homopolymer of monomer (**4a**) in the nematic phase where the laterally affixed mesogens are parallel to the backbone had a prolate extended shape with the radius of gyration of 75 Å along the backbone and 15 Å perpendicular to the backbone. In the isotropic phase the radius of gyration was 35 Å. This implies that the backbone is in a coiled conformational state in the isotropic phase compared to the more extended, wormlike, state in the nematic phase. This change in the backbone's extension from a wormlike to coiled state due to the conformational changes occurring for LCE 1 and LCE 2 through the nematic to isotropic phase transition explains qualitatively the reason for the contraction (extension) observed on heating (cooling).

Isostrain measurement was carried out on LCE 1 and LCE 2 by maintaining a constant strain on the film along the rubbing direction and measuring the force generated as a function of temperature (Figure 5). Maximum retractive force developed in the film as it is heated through the nematic to isotropic phase transition was determined by holding the film at constant length with a known strain imposed on it. The initial strain applied to the films at the lowest temperature studied was low, ~5% for both LCE 1 and LCE 2. The maximum retractive force generated at the highest temperature in LCE 1 and LCE 2 was 210 and 270 kPa, respectively. Because the development of retractive stress during the isostrain measurement is related to the entropy change, it can be understood conformationally as a result of the initial work of the wormlike to coil transition observed in backbones with laterally coupled liquid crystal side chains. It can be inferred from the greater retractive stress observed in LCE 1 than in LCE 2 through the phase transition, having slopes of 0.012 MPa/°C for LCE 1 and 0.0085 MPa/°C for LCE 2, that a larger change in conformational states occurs for LCE 1 than in LCE 2. LCE 2 may have a reduced retractive stress because of the reduced orientational order of the mesogens with flexible cyclohexane groups. The measurement of the retractive stress at constant temperature has been a classical method in order to measure the conformational entropy as a function of length change for elastomers.[29,30] This measurement demonstrates that the material behaves as an elastomer and confirms that upon passing through the nematic to isotropic phase transition the elastomer develops internal stress. This internal stress is classically related to the spring constant α of the network[29,30] via the thermodynamic equations of state, $[dF/dT]_l = -[dS/dl]_T = \alpha$, where F is the static force applied, T the temperature, l the length of the elastomer, S the entropy, and α a constant. The slope of the static force vs temperature curve is small in the nematic phase and shows a sharp increase around the nematic to isotropic phase transition. The increase in the slope is consistent with the increase in entropy on going from the nematic to isotropic phase transition. The slope of the linear portion of the stress vs temperature plot in the nematic phase is ~0.001 MPa/°C, which was determined at temperatures below 70 °C, for LCE 2 whereas the value in the isotropic phase is 0.0019 MPa/°C, which was determined at temperatures higher than 105 °C. The larger slope in the nematic to isotropic phase transition region can be explained as follows. Even though the initial stress applied to the film in the nematic phase is only ~5%, the film, which would like to contract on going over to the isotropic phase, experiences an additional strain equal to the strain observed in the film during thermoelastic studies (see Figures 3

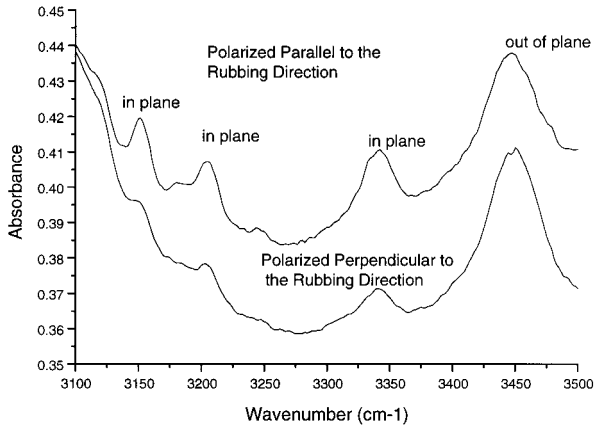

Figure 6. Polarized FTIR spectra in the region of the C═C overtone of the aromatic in-plane stretch at 3343 cm^{-1}. The top (bottom) curve is for the polarization parallel (perpendicular) to the rubbing direction.

and 4). The step change between 114 and 121 °C for LCE 1 and between 76 and 95 °C for LCE 2 is related to the phase change. The dF/dT value in this transition region is 0.012 MPa/°C for LCE 1 and 0.0085 MPa/°C for LCE 2. These values are orders of magnitude higher than typical dF/dT values of vulcanized rubber, which have values ranging from −0.000 156 8 to 0.000 63 MPa/°C with isostrains from 3% to 38%, respectively.[31]

The change in the order parameter, S, of the liquid crystal mesogens through the liquid crystalline to isotropic phase transition on cooling was determined using polarized FTIR spectroscopy. The transition dipole moment that was used for the determination of the order parameter was a C═C overtone of the aromatic in-plane stretch at 3343 cm^{-1}. The order parameter was determined by generating a polar plot of the peak height at 3343 cm^{-1} as a function of the angle between the polarization axis and the rubbing direction. Figure 6 shows that the chosen overtone and its neighboring baseline region allowed for the calculation of dichroic ratios. The dichroic ratio R, ratio of absorbance parallel to rubbing direction to absorbance perpendicular to rubbing direction, could be determined accurately from the polar plots. The order parameter was calculated from the well-known expression[32,33] $S = (R - 1)/(R + 2)$, where S is the order parameter and R is the dichroic ratio.

Representative polar plots for the mixture of monomer **4a** with the cross-linker before polymerization and for the elastomers LCE 1 and LCE 2 are shown in Figure 7a−c. The order parameter, S, for the monomer mixture at room temperature was found to be 0.57 ± 0.02. The aligned LCEs have less order than the monomer and cross-linker mixture, as seen by the polar plots. The order parameters, as determined from such polar plots, as a function of temperature for the two elastomer films are shown in Figures 8 and 9. Error in the order parameter is mainly due to the baseline noise of ±0.001 Abs and was estimated from repeated scans. The maximum value of S measured for the two films is 0.33 ± 0.04 and 0.28 ± 0.04 respectively for LCE 1 and LCE 2. The order parameter decreases sharply near the N−I transition. However, the value of S does not go to zero but retains a finite value due to the network. This has been observed in mechanically oriented liquid crystalline elastomeric systems and has been referred as "paranematic".[34] The presence of the "paranematic" phase suggests that the residual anisotropy is associated with the anisotropy left over in the network, and it may be an indication of the amount of the residual order in the network. The higher remnant order in the isotropic phase of LCE 1 than in LCE 2 suggests a stronger coupling of the network to the LC mesogens. The variation of the order parameter near NI is sharper in LCE 1 compared to LCE 2. This behavior is consistent with the sharpness differences in the thermoelastic behavior of the two elastomers. Figure 10 shows a combined plot of the strain and order parameter variation with temperature. This plot illustrates the correlation between the microscopic molecular order and the macroscopic film response.

The relaxation behavior of dynamic mechanical shear deformations in LCE 1 is shown in Figures 11 and 12, the loss modulus and tan δ, over a temperature range near the isotropic to nematic phase transition. The increase in tan δ with frequency indicates the existence of a peak above 100 Hz. Since the loss modulus values are small below 10 Hz, contributions of low-frequency viscous relaxations appear to be minimal, and the elastomer exhibits mostly elastic behavior. The dynamic mechanical behavior shows that the relaxation would not be hindered by lower relaxation frequencies associated with the glass transition. The response times of the material with respect to mechanical deformations appear to be limited by the relaxations of the polymer network. Lower frequency relaxations associated with softening of the backbone begin appearing at temperatures below the nematic to isotropic phase transition. Earlier dielectric studies[35] on LCE 1, which showed the

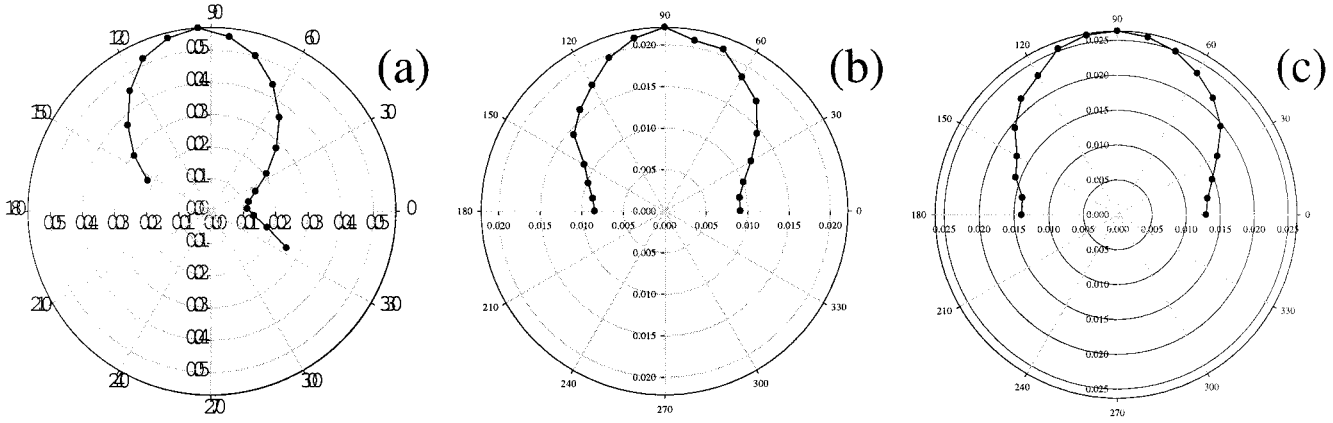

Figure 7. Representative polar plots of (a) monomer **4a** at 25 °C, (b) LCE 1 at 116 °C, and (c) LCE 2 at 78 °C.

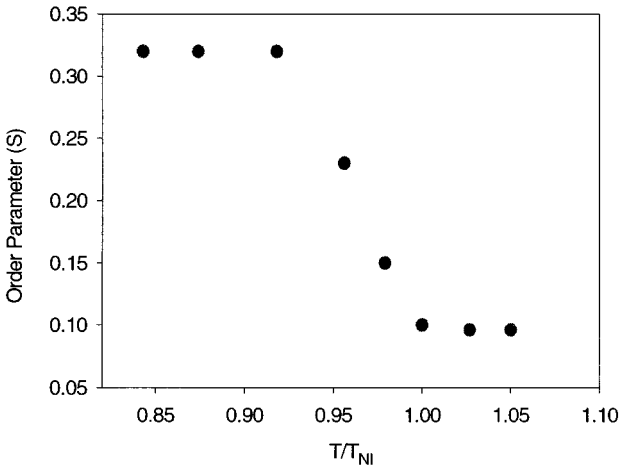

Figure 8. Plot of the order parameter as a function of reduced temperature (T/T_{NI}) through the isotropic to nematic phase transition for LCE 1. T_{NI} is the nematic−isotopic phase transition temperature.

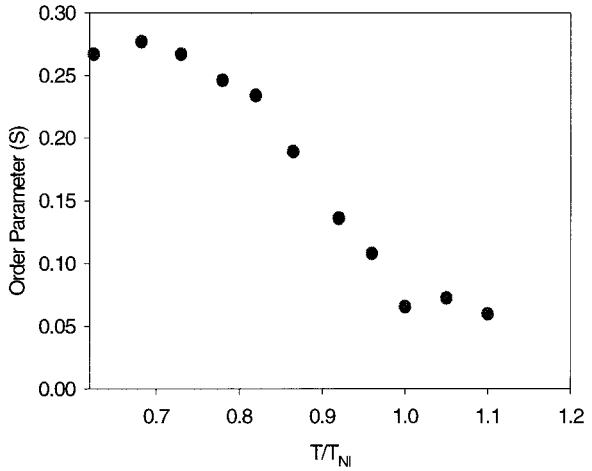

Figure 9. Plot of the order parameter as a function of reduced temperature (T/T_{NI}) through the isotropic to nematic phase transition for LCE 2. T_{NI} is the nematic−isotopic phase transition temperature.

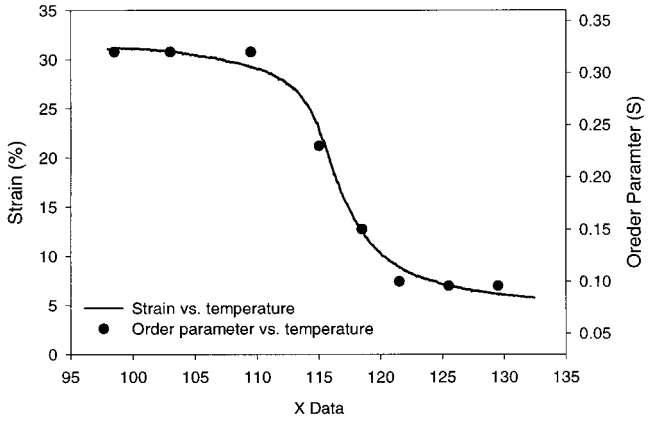

Figure 10. Combined plot of strain and order parameter measurements for LCE 1. The thermoelastic curve was obtained at a heating/cooling rate of 0.5 °C.

presence of a molecular relaxation associated with the side chain liquid crystalline mesogen above 100 Hz, indicated that the reorientation of the liquid crystal groups is not the limiting factor. Since the losses are minimal below 10 Hz, we expect the mechanical strain response to be in the ∼100 ms regime.

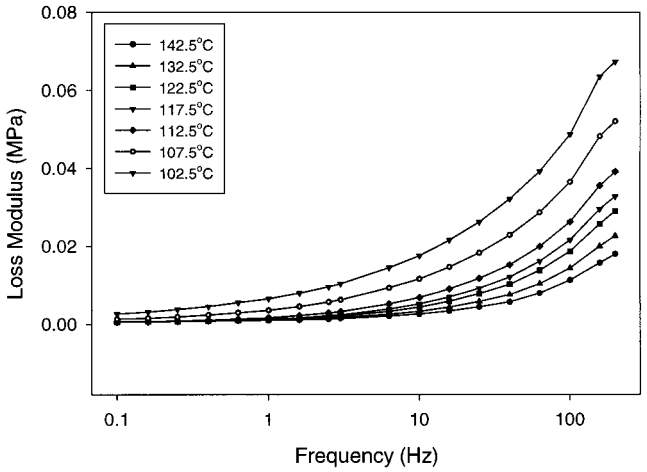

Figure 11. Plot of loss modulus as a function of frequency at different temperatures for LCE1.

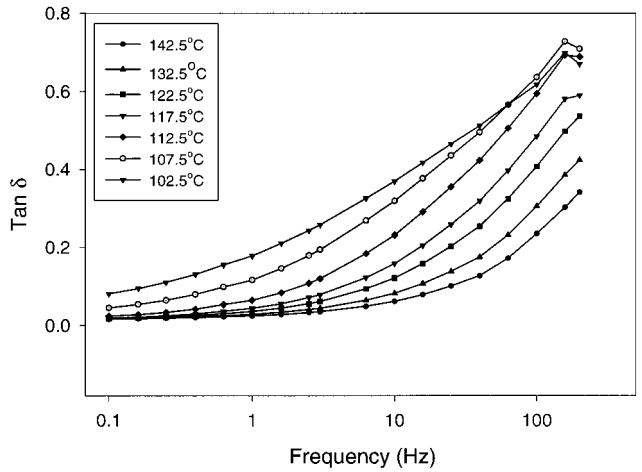

Figure 12. Plot of tan δ as a function of frequency at different temperatures for LCE1.

Conclusions

We have shown in this paper that nematic liquid crystalline elastomers can exhibit muscle-like physical properties with stresses of 210 kPa, strains of 35−45%, and subsecond relaxations through the nematic to isotropic phase transition. The entropic origin of the mechanical response is due to the loss of side chain mesogenic order through the nematic to isotropic phase. This loss of order at the phase transition imposes a change in the conformational entropy of the backbone from a wormlike to a coiled conformational state leading to a step change in the elastic retractive force as a function of temperature. A detailed understanding of this entropic mechanism can lead to exciting possibilities in designing this class of artificial muscle actuators.

Acknowledgment. The authors acknowledge financial support from DARPA Controlled Biological and Biomimetic Systems Program. D.L.T. thanks NAS for his NRC Postdoctoral Research Fellowship. The authors thank Dr. David Holt for helpful discussions.

References and Notes

(1) Pennycuick, C. J. *Newton Rules Biology: A Physical Approach to Biological Problems*; Oxford University Press: New York, 1992.

(2) Uchino, K. *Ceram. Bull.* **1986**, *65*, 647−652.

(3) Hunter, I. W.; Lafontaine, S.; Hollerbach, J. M.; Hunter, P. J. *IEEE* **1991**, 166−170.
(4) Baughman, R. H.; Shacklette, L. W.; Elsenbaumer, R. L.; Plichta, E. J.; Becht, C. In *Conjugated Polymeric Materials: Opportunities in Electronics, Optoelectronics, and Molecular Electronics*; Bredas, J. L., Chance, R. R., Eds.; Kluwer: Dordrecht, The Netherlands, 1990; Vol. 1990, pp 559−582.
(5) Smela, E.; Inganas, O.; Lundstrom, I. *Science* **1995**, *268*, 1735.
(6) Kaneto, K.; Kaneko, M.; Min, Y.; MacDiarmid, A. G. *Synth. Met.* **1995**, *71*, 2211.
(7) Pelrine, R.; Kornbluh, R.; Pei, Q.; Joseph, J. *Science* **2000**, *287*, 836−839.
(8) Baughman, R. H.; Cui, C.; Zakhidov, A. A.; Iqbal, Z.; Barisci, J. N.; Spinks, G. M.; Wallace, G. G.; Mazzoldi, A.; De Rossi, D.; Rinzler, A. G.; Jaschinski, O.; Roth, S.; Kertesz, M. *Science* **1999**, *284*, 1340−1344.
(9) Liu, Z.; Calvert, P. *Adv. Mater.* **2000**, *12*, 288−291.
(10) Hunter, I. W.; LaFontaine, S. *Technol. Dig. IEEE Solid-State Sens. Actuat. Workshop* **1992**, 178−185.
(11) Gleim, W.; Finkelmann, H. *Makromol Chem* **1987**, *188*, 1489−1500.
(12) de Gennes, P.-G. *C. R. Acad. Sci. Paris, Ser. II* **1997**, *324*, 343−348.
(13) Gleim, W.; Finkelmann, H. In *Side Chain Liquid Crystalline Polymers*; McArdle, Ed.; Blacktie and Son Ltd: Glasgow, 1989; pp 287−308.
(14) Zentel, R. *Adv. Mater.* **1989**, 321−329.
(15) Davis, F. J. *J. Mater. Chem.* **1993**, *3*, 551−562.
(16) Brand, H. R.; Finkelmann, H. In *Physical Properties of Liquid Crystalline Elastomers*; Demus, D., Ed.; Wiley VCH: New York, 1998; pp 277−302.
(17) Terentjev, E. M. *J. Phys.: Condens. Matter* **1999**, *11*, R239−R257.
(18) Kupfer, J.; Finkelmann, H. *Makromol. Chem., Rapid Commun.* **1991**, *12*, 717−726.
(19) Kundler, I.; Finkelmann, H. *Macromol. Chem. Phys.* **1998**, *199*, 677−686.
(20) Legge, C. H.; Davis, F. J.; Mitchell, G. R. *J. Phys. II* **1991**, *1*, 1253−1261.
(21) Keller, P.; Carvalho, B.; Cotton, J. P.; Lambert, M.; Moussa, F.; Pepy, G. *J. Phys., Lett.* **1985**, *46*, L1065.
(22) Leroux, N.; Keller, P.; Achard, M. F.; Noirez, L.; Hardouin, F. *J. Phys. II* **1993**, *3*, 1289−1296.
(23) Hardouin, F.; Leroux, N.; Mery, S.; Noirez, L. *J. Phys. II* **1992**, *2*, 271−278.
(24) Kirste, R. G.; Ohm, H. G. *Makromol. Chem., Rapid Commun.* **1985**, *6*, 179.
(25) Mattoussi, H.; Ober, R.; Veyssie, M.; Finkelmann, H. *Europhys. Lett.* **1986**, *2*, 233.
(26) Arrighi, V.; Higgins, J. S.; Weiss, R. A.; Cimecioglu, A. L. *Macromolecules* **1992**, *25*, 5297−5305.
(27) D'Allest, J. F.; Maissa, P.; ten Bosch, A.; Sixou, P.; Blumstein, A.; Blumstein, R.; Teixeira, J.; Noirez, L. *Phys. Rev. Lett.* **1988**, *61*, 2562−2565.
(28) The hysteretic width was found to decrease with decreasing heating/cooling rate, and the width was zero for rates below 1.5 °C.
(29) Flory, P. J. *Principles of Polymer Chemistry*; Cornell University Press: Ithaca, NY, 1953.
(30) Alkonis, J. J.; Macknight, W. J. *Introduction to Polymer Viscoelasticity*, 2nd ed.; John Wiley and Sons: New York, 1983.
(31) Anthony, R. L.; Caston, R. H.; Guth, E. *J. Phys. Chem.* **1942**, *46*, 826.
(32) Buerkle, K.-R.; Frank, W. F. X.; Stoll, B. *Polym. Bull.* **1988**, *20*, 549.
(33) Sahlen, F.; Andersson, H.; Hult, A.; Gedde, U. W.; Ania, F. *Polymer* **1996**, *37*, 2657−2662.
(34) Schatzle, J.; Kaufhold, W.; Finkelmann, H. *Makromol. Chem.* **1989**, *190*, 3269−3284.
(35) Shenoy, D.; Filippov, S.; Aliev, F.; Keller, P.; Thomsen, D.; Ratna, B. *Phys. Rev. E* **2000**, *62*(6), 8100.

MA001639Q